High-performance multiblock PEMs containing a highly acidic fluorinated-hydrophilic domain for water electrolysis

Lee, Kwan-Soo
Chae, Ji Eon
Lee, So Young
Baek, Sae Yane
Song, Kwang Ho
Park, Chi Hoon
Kim, Hyoung-Juhn

To be published in: Journal of Membrane Science

DOI to publisher's version: 10.1016/j.memsci.2021.119694

High-performance multiblock PEMs containing a highly acidic fluorinated-hydrophilic domain for water electrolysis

Ji Eon Chae[a,b,1], So Young Lee[a,c,1], Sae Yane Baek[a], Kwang Ho Song[b], Chi Hoon Park[c,d], Hyoung-Juhn Kim[a,*], Kwan-Soo Lee[c,*]

[a] *Center for Hydrogen·Fuel Cell Research, Korea Institute of Science and Technology (KIST), Hwarang-ro 14-gil 5, Seongbuk-gu, Seoul 02792, Republic of Korea*

[b] *Department of Chemical and Biological Engineering, Korea University, Anam-ro 145, Seongbuk-gu, Seoul 02841, Republic of Korea*

[c] *C-CDE: Chemical Diagnostics and Engineering, Los Alamos National Laboratory, Los Alamos, New Mexico 87545, USA*

[d] *Department of Energy Engineering, Gyeongsang National University, Jinju-si 52725, Republic of Korea*

[*]Corresponding authors

Dr. Kwan-Soo Lee

Tel.: +1–505–667–3060, e-mail: kslee@lanl.gov

Dr. Hyoung-Juhn Kim

Tel.: +82–2-958–5299, fax: 82–2-958–5199, e-mail: hjkim25@kist.re.kr

Abstract

The present paper describes the design and evaluation of novel hydrophilic–hydrophobic poly(arylene ether sulfone) (PAES) multiblock copolymers for their synergistic effects upon transport properties and their potential use in proton exchange membrane water electrolysis. The multiblock copolymers are prepared via a coupling reaction between (i) a hydrophilic segment consisting of a disulfonated quinone fluorinated biphenyl group that contains fluorine moieties next to the sulfonated groups to increase the acidity, and (ii) hydrophobic segments composed of non-sulfonated biphenyl sulfone to provide dimensional stability. Two different lengths (molecular weights; 5k and 10k, where k represents 10^3 g mol^{-1}) of hydrophobic segments are used to investigate the effects of the membrane properties compared with those of Nafion® and PAES random copolymer (i.e., BPSH40). Atomic force microscopy images of the BPSH40 and multiblock membranes are shown to agree closely with a mesoscale simulation, thus confirming the importance of the morphological effect upon the transport properties. Moreover, the multiblock copolymer with a higher proportion of hydrophilic segments (10k–5k) was shown to provide enhanced performance (3.41 A cm^{-2} at 1.9 V) compared to the multiblock copolymer with equal proportions of hydrophilic and hydrophobic segments (10k–10k) due to the greater continuity of nano-sized ionic channels.

Keywords: Multiblock copolymer, Proton exchange membrane water electrolysis, Phase separation, Morphology, Mesoscale simulation

1. Introduction

Hydrogen (H_2) is a promising future energy carrier or fuel with a high energy density per unit mass relative to other energy storage materials such as methane, diesel, and several types of battery [1]. Although water electrolysis (WE) is an eco-friendly technology for producing high-purity H_2, the cost of electricity needed for water splitting has impeded its large-scale development. The most economically viable way to produce H_2 while reducing fossil fuel consumption and CO_2 emissions would use renewable energy sources such as solar panels and wind turbines, referred to as the "power-to-gas" approach. Due to its high current density, proton exchange membrane water electrolysis (PEMWE) is the only technology with a sufficiently fast transaction for coupling with renewable energy production devices and is a relatively compact electrolysis technology [2, 3]. Thus, H_2 production via the PEMWE process using emission-free renewable power sources holds promise for advancing the emerging hydrogen economy and promoting its efficiency and economic viability in the near future. However, the cost of PEMWE system components and materials must be overcome.

The principle of PEMWE operation is that the water supplied to the anode is oxidized by a catalyst such as iridium (IV) oxide (IrO_2) to separate the protons (H^+) and electrons and, thus, generate oxygen (O_2) gas. The generated H^+ ions pass to the cathode along the proton exchange membrane (PEM) and react with electrons to produce hydrogen gas (H_2), as shown schematically in Figure 1a. In the PEMWE system, the PEM functions as a proton conductor for H_2 production and as a separator for preventing the crossover of the different gases generated on each side, thus significantly impacting its performance and safety. Therefore, the long-term durability of the system requires the PEM to exhibit high proton conductivity and low gas crossover properties, high chemical resistance, and superior dimensional stability in a full hydration environment.

In practice, perfluorinated sulfonic acid (PFSA) ionomer membranes such as Nafion, Aciplex, or Flemion, which are composed of a polytetrafluoroethylene backbone and a randomly tethered ionic group (SO_3^-) as a side-chain, have been widely used as polymer electrolyte materials for more than 30 years due to their excellent chemical resistance, mechanical toughness, and high proton conductivity [4]. However, their high fuel permeabilities, high cost, complicated synthetic procedure, low glass transition temperature (T_g), and negative environmental impact limit their further application and commercialization [5, 6]. Therefore, a significant effort has been devoted to research into hydrocarbon-based polymer electrolytes as effective alternatives to PFSAs, offering high chemical and thermal stability and lower material cost, along with enhanced mechanical stability and environmental friendliness [5–13].

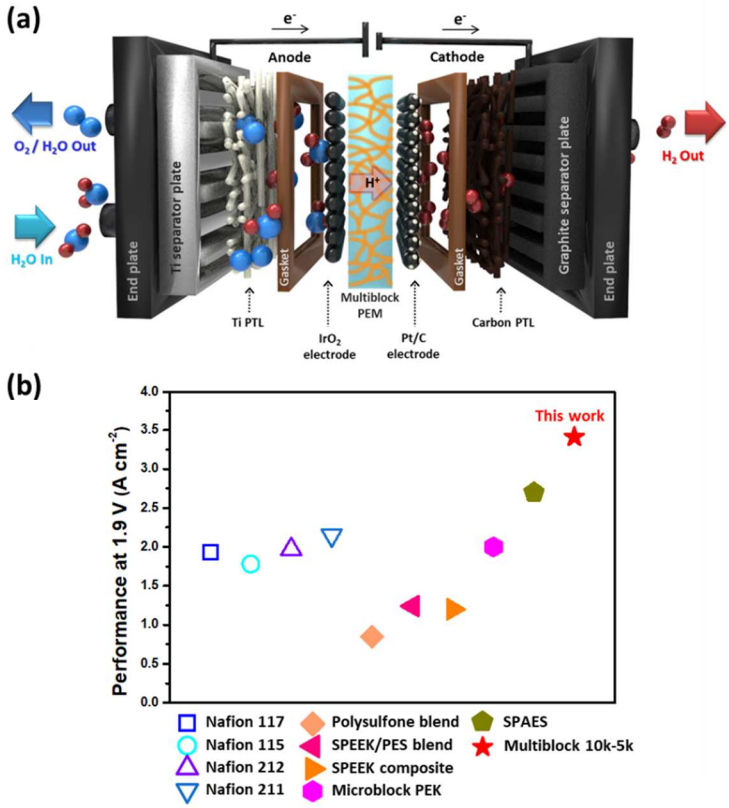

Figure 1. (a) A schematic diagram of the PEMWE, and (b) a wider comparison including previously-reported hydrocarbon and PFSA-based PEMs [7–9, 14–18].

Of the various hydrocarbon-based polymer electrolytes, the poly(arylene ether)s (PAEs) have been extensively investigated due to their potential advantages, such as excellent chemical and thermal stability and low fuel permeability. However, these polymers have relatively lower proton conductivity and durability compared to the PFSAs. Many researchers have attempted to overcome these issues by making various modifications to the PAE PEMs. For instance, polar or functional groups such as nitrile, fluorine, and phosphine were introduced into the polymer structure to improve the transport properties of membranes [19–21]. However, there were limitations in creating well-defined ion channels and increasing the ion-exchange capacity (IEC) due, primarily, to the inherent chemical structure of the PAE polymers. Specifically, these are copolymers in which the sulfonated groups are randomly distributed along the polymer chains, thus resulting in a decrease in connectivity between the ion channels. Attempts to solve this structural issue have included the design of well-defined morphological structures via modification with locally densified sulfonated polymer systems, chemical cross-linking systems, hydrophilic–hydrophobic multiblock copolymer systems, and side-chain fluoro-alkylated polymer systems [19, 22–29]. For instance, McGrath et al. have reported the development of a hydrophilic-hydrophobic multiblock copolymer with good connectivity between hydrophilic domains, excellent phase separation between the hydrophilic and hydrophobic domains even at low relative humidity, and a higher water diffusion coefficient than that of random copolymers and Nafion [24, 25, 29–33]. This morphology of multiblock copolymer improves proton conductivity by providing well-formed ionic channels [34] and decreasing the dependency of the transport properties upon the relative humidity [24]. To promote greater phase separation, McGrath et al. also designed the fluorinated decafluorobiphenyl (DFBP) and hexafluorobenzene (HFB) linkage groups for use as hydrophilic and hydrophobic oligomers and demonstrated that the fluorine-enriched DFBP linkage induces a nano-phase-separated morphology [30]. These results confirm that

well-defined ionic channels are necessary for improved ion transport properties in PEMs.

As well as the chemical and morphological modification of hydrocarbon-based PEMs, studies to enhance the acidity of PEMs have been conducted. For example, Bae et al. prepared hydrocarbon-based PEMs composed of the same primary polymer chain with various side chains such as fluoroalkyl sulfonic acid, aryl sulfonic acid, and alkyl sulfonic acid, to evaluate the effect of acidity on the transport properties [35, 36]. The fluoroalkyl sulfonated PEM exhibited excellent transport properties compared with those of the alkyl and aryl sulfonated PEMs, despite its low water uptake and IEC. Furthermore, an investigation of the pK_a values of simple sulfonic acid molecules also confirms the effect of acidity: for example, the pK_a values of benzene sulfonic acid (one of the aryl sulfonic acids) and methane sulfonic acid (one of the alkyl sulfonic acids) are approximately −2.5 and −2.0, respectively, while the pK_a of trifluoromethanesulfonic acid (one of the fluoroalkyl sulfonic acids) is approximately −13.0 [37].

In the present study, a new type of PAE-based multiblock copolymer is synthesized, and its transport properties and PEMWE performance are evaluated. A sulfonated-fluorinated segment of this multiblock copolymer is designed as a hydrophilic block in order to achieve the following three primary attributes: (1) sufficient acidity of the hydrophilic block, (2) a well-defined morphological structure with the formation of ionic channels, and (3) a low fuel permeability. The length of each hydrophilic and hydrophobic segment is shown to influence the phase separation morphology of the multiblock membrane directly. Furthermore, the mechanism by which this morphology affects the transport properties is investigated using atomic force microscopy (AFM) and mesoscale simulation. Thus, the membrane characteristics, morphologies, transport properties, gas permeabilities, and water electrolysis performances of two synthesized multiblock copolymers with different IECs are evaluated

and compared with those of a random sulfonated poly(arylene ether sulfone) (BPSH40) [38] and Nafion 212.

2. Experimental

2.1. Materials

Potassium 2,5-dihydroxybenzene-1,4-disulfonate (DSHQ) was purchased from Acros Organics; decafluorobiphenyl (DFBP), 4,4'-dichlorodiphenylsulfone (DCDPS), 4,4'-diphenol (BP), and potassium carbonate were purchased from Aldrich Chemical Co. and used after vacuum drying at 100 °C for two days. Anhydrous dimethyl sulfoxide (DMSO), *N,N'*-dimethylacetamide (DMAc), toluene, and cyclohexane were purchased from Aldrich Chemical Co. and used without further purification.

2.2. Synthesis of oligomers

2.2.1. The hydrophilic disulfonated quinone fluorinated biphenyl (DSQFBP) oligomer

The hydrophilic disulfonated quinone fluorinated biphenyl (DSQFBP) oligomer was synthesized via the step-growth polymerization [31] of DSHQ with DFBP, as indicated in Figure 2a. The molecular weight (M_n) of the oligomer was controlled by the monomer feed ratio [39]. For example, the synthesis of the oligomer with an M_n of 10,000 g mol^{-1} proceeded as follows: DSHQ (10.0 g, 28.8667 mmol), DFBP (10.3056 g, 30.845 mmol), and K_2CO_3 (4.7876 g, 1.2 eq.) in 2:1 DMSO/ toluene (80 mL:40 mL) was placed in a 250 mL three-necked round-bottomed flask equipped with a mechanical stirrer, a nitrogen inlet, and a Dean-Stark trap. The reaction mixture was heated to 120 °C for 5 h with refluxing toluene in the Dean-Stark trap to ensure complete dehydration. After 5 h, the toluene was removed by slowly increasing the temperature to 150 °C. The reaction was allowed to proceed for a

further period of 48 h. The resulting viscous solution was then cooled to room temperature and precipitated in isopropyl alcohol. Finally, the oligomer was dried at 120 °C in a vacuum oven for at least 24 h.

2.2.2. The hydrophobic biphenyl sulfone (BPS) oligomer

The hydrophobic biphenyl sulfone (BPS) oligomer was synthesized via nucleophilic step-growth polymerization, as indicated in Figure 2b. The synthesis of the oligomers with M_n values of 5,000 and 10,000 g mol^{-1} proceeded as previously described in the literature [32].

2.3. Synthesis of multiblock copolymers (DSQFBP-BPS)

The multiblock copolymers were synthesized via a coupling reaction between a DFBP-terminated hydrophilic oligomer and a phenoxide-terminated BPS hydrophobic oligomer, as indicated in Figure 2c. In brief, the DSQFBP, BPS, K_2CO_3, anhydrous DMAc, and cyclohexane were added to a 250 mL three-necked round-bottomed flask equipped with a mechanical stirrer, a nitrogen inlet, and a Dean-Stark trap. The reaction mixture was heated to 100 °C with refluxing cyclohexane in the Dean-Stark trap to ensure complete dehydration. After 4h, the cyclohexane was removed without increasing the temperature and the reaction was allowed to proceed for a further 5 h. The obtained multiblock copolymer was precipitated into isopropyl alcohol/water (8:2 v/v), filtered, and dried in a vacuum oven at 100 °C for at least 24 h.

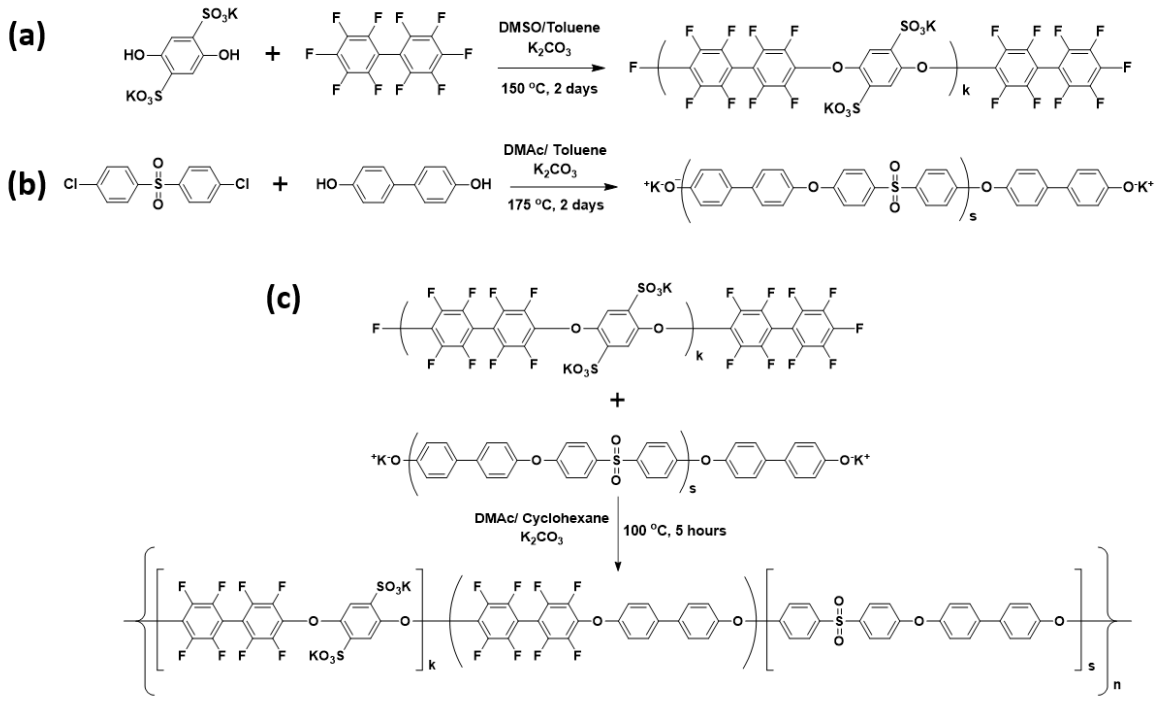

Figure 2. Schematic synthesis of (a) the hydrophilic oligomer, (b) the hydrophobic oligomer, and (c) the multiblock copolymer.

2.4. Membrane preparation

The membrane was prepared via the solvent casting method. Hereafter, the obtained multiblock copolymers are denoted as 10k–5k and 10k–10k, where k represents 10^3 g mol^{-1}, according to the M_n of the hydrophilic–hydrophobic oligomers. Each multiblock copolymer (10k–5k and 10k–10k) and the random copolymer (BPSH40) were fully dissolved in DMAc to a concentration of 5 wt.% at 50 °C. The polymer solution was then filtered with a 0.45-μm Teflon syringe filter, poured onto a flat glass plate, and dried thoroughly in a vacuum oven. The membranes were immersed in 1 M aqueous sulfuric acid at 80 °C to replace the potassium ions with protons. Finally, the membrane was prepared by washing several times to remove the excess protons, then drying thoroughly.

2.5. Polymer characterization

2.5.1. Nuclear magnetic resonance (NMR) spectroscopy

The proton (^{1}H) and fluorine-19 (^{19}F) nuclear magnetic resonance (NMR) analyses were conducted on a Varian INOVA 400 MHz spectrometer with DMSO-d6 to confirm the chemical structures of the oligomers and multiblock copolymers and to determine the copolymer compositions and M_n of the oligomers via end-group analysis.

2.5.2. Intrinsic viscosity (IV)

The intrinsic viscosities (IVs) of the oligomers and multiblock copolymers were obtained via size-exclusion chromatography (SEC) using a Waters 1515 isocratic HPLC pump, a Waters autosampler, a Waters HR5-HR4-HR3 column set, a Waters 2414 refractive-index detector, and a Viscotek 270 detector, with N-methyl-2-pyrrolidinone (NMP) containing 0.05 M LiBr at 60 °C as the mobile phase [40].

2.5.3. Ion exchange capacity (IEC), water uptake, swelling ratio, and proton conductivity

The ion exchange capacity (IEC) was determined using a titration method. The membranes were first acidified, washed, then dried at 80 °C in a vacuum oven for 24 h. The dried membranes were then immersed in a 0.1 M NaCl solution for 48 h to replace H^+ with Na^+. The remaining liquid was titrated with a 0.1 M NaOH solution using phenolphthalein as an indicator. The IEC values were expressed in units of meq. ($-SO_3H$)/g of the dry membrane and were obtained using Eq. (1):

$$\text{IEC (meq. g}^{-1}) = \frac{consumed\ NaOH \times molarity\ NaOH}{Weight\ of\ dried\ membrane} \quad (1)$$

The water uptake and swelling ratio measurements of each membrane were performed on 1 × 6 cm samples. The measurements were conducted by the change in weight and volume of

the membranes before and after immersing in deionized water at room temperature and high temperature (90 °C). First, the membranes in the acid form were dried at 80 °C in a vacuum oven for 24 h, then their weight was recorded. The membranes were then soaked in deionized water for 48 h at room temperature. The water was lightly removed from the surfaces of the wet membranes, then their weight, length, and thickness were measured. For the measurements under high-temperature, the wet membranes were immersed in boiling water at 90 °C for 5 h. The water droplets were quickly removed from the membranes, which were then weighed. The water uptake and in-plane (Δl) and through-plane (Δt) swelling ratios were calculated using Eqns. (2–4):

$$\text{Water uptake } (\%) = \frac{W_{wet} - W_{dry}}{W_{dry}} \times 100 \quad (2)$$

where W_{wet} is the weight of the wet membrane, and W_{dry} is the weight of dried membrane;

$$\text{Swelling ratio, } \Delta l\ (\%) = \frac{L_{wet} - L_{dry}}{L_{dry}} \times 100 \quad (3)$$

and

$$\text{Swelling ratio, } \Delta t\ (\%) = \frac{t_{wet} - t_{dry}}{t_{dry}} \times 100 \quad (4)$$

where L_{wet} and t_{wet} are the length and thickness of the wet membrane, and L_{dry} and t_{dry} are the length and thickness of the dry membrane. These ratios were determined from the dimensional changes from the wet to the dry state.

The proton conductivity (σ, S cm^{-1}) of each membrane sample (1 × 4 cm) was obtained by measuring its resistance in deionized water at 30 and 90 °C using the four-electrode method in contact with the membrane surface (the in-plane direction) under alternating current (AC). A four-point probe AC impedance spectroscopy system was used (SP-300, BioLogic Science Instruments). The impedance of the membrane was measured in a controlled humidity and

temperature chamber via the Nyquist plot. The conductivity was calculated using Eq. (5):

$$\text{Proton conductivity (S cm}^{-1}) = \frac{L}{R \times A} \quad (5)$$

where L (cm) is the distance between the working electrode and the reference electrode, A (cm^2) is the cross sectional area of the membrane, and R (Ω) is the membrane resistance.

2.5.4. Thermalgravimetric analysis (TGA)

The thermal degradation (T_d) was determined by thermalgravimetric analysis (TGA) in the range of 40 to 800 °C at a heating rate of 10 °C min^{-1} under a nitrogen atmosphere using a Q50 machine (TA Instruments). The multiblock copolymer membranes were analyzed in proton form, and each sample was prepared with a weight of approximately 10 mg. All samples were preheated at 150 °C for 1 h to remove moisture.

2.5.5. Atomic force microscopy (AFM)

Tapping mode AFM was performed using a Veeco Multimode Atomic Force Microscope. Samples were equilibrated at 40% RH at room temperature for at least 24 h and sealed before imaging.

2.6. Gas permeability

Gas permeabilities of each membrane were measured using both time-lag method at 30 °C and the pressure decay method at high temperature and high pressure. First, the H_2 and O_2 permeability of each membrane was investigated by the time-lag method which measures the downstream pressure by the gas passing through the membrane at a constant volume. The membrane was loaded into the time-lag test cell (effective area: 15.20 cm^2) with a measurement temperature of 30 °C. The pressure of the feed side filled with dry gas was set to 1010 torr, and the gas permeability through the membrane was calculated from Eq. (6):

$$\text{P} = \frac{V \times T_0 \times l}{p_0 \times T \times \Delta p \times A} \times \frac{dp}{dt} \quad (6)$$

where P is the gas permeability in Barrer (1 Barrer = 10^{-10} cm^3 (STP) cm (cm^{-2} s^{-1} cm Hg^{-1})), V is the volume of the permeate chamber in cm^3, l is the membrane thickness in cm, A is the effective area in cm^2, T_0 is the standard temperature in Kelvin (K), p_0 is the feed pressure in cm Hg, T is the setup temperature in K, Δp is the pressure difference between the feed and permeate of the membrane (cm Hg), and dp/dt is the slope plotted from the increase in permeated pressure over time.

Also, the H_2 permeability was measured using the pressure decay method at both 30 and 90 °C. The membrane was loaded into a testing cell (effective area: 12.57 cm^2). The buffer tank was filled with H_2 and pressurized to 15 bar. Then, at each set temperature, H_2 was slowly fed to the testing cell up to 10 bar. The pressure over time was recorded on a pressure sensor connected to the testing cell, and the data were calculated for the H_2 permeability in the manner reported by Kim et al. [41].

2.7. Fabrication of the membrane electrode assembly (MEA)

The catalyst slurry for the O_2 electrode (anode) was composed of a mixture of IrO_2 (99.99%, Alfa Aesar), a PFSA ionomer (DE-520, Dupont), deionized water, and 2-propanol (Honeywell). For the H_2 electrode (cathode) catalyst slurry, the catalyst Pt/C (46.2 wt.%, Tanaka) was used in place of the IrO_2. The ionomer content was fixed at 30 wt.% for both the anode and cathode in all samples. The catalyst slurry mixtures were dispersed using bath sonication. Each catalyst slurry was spray-coated onto both sides of the membrane via the catalyst-coated membrane (CCM) method. The active area of each membrane electrode assembly (MEA) was 4 cm^2. The IrO_2 and Pt loadings were 1.0 and 0.4 mg cm^{-2}, respectively. Titanium (Ti) felt (2GDL09N-025, Bekaert, 290 μm) was used as a porous transport layer (PTL) for the anode. The Ti felt was enabled to remove TiO_2 with pretreatment in 5% oxalic acid dehydrate solution (Daejung). In addition, non-woven carbon paper gas diffusion

medium Sigracet SGL 39BC (SGL carbon Inc., 340 μm) was used as a PTL for the cathode. The catalyst-coated membranes were sandwiched with PTLs and Teflon gaskets. Separator plates at the anode and cathode were Ti and graphite, respectively. Finally, the MEA was assembled as a single cell.

2.8. Evaluation of the WE performance

The WE performance was tested in a water electrolysis test station (CNL-SPEL, CNL). The current-voltage polarization curves of the MEAs were obtained by loading the stepwise cell voltage from 1.35 to 2 V at 90 ℃. The water temperature of the anode was set to 60 ℃, and the water was supplied to the anode at 15 ml min^{-1}. The cathode inlet was blocked to ensure the dry condition.

2.9. Mesoscale simulation

The MesoDyn module in the Materials Studio program package (Biovia) which is based on dynamic mean-field density functional theory [42, 43], was used for mesoscale simulation in this study. Hydrophilic repeating units were represented as the “L” bead in the multiblock copolymers (10k–5k and 10k–10k) and the “BL” bead in the random copolymer (BPSH40), respectively. For the hydrophobic repeating unit, the “P” bead was used for all copolymer models due to their identical chemical structure. The Gaussian chain models of the copolymers were composed of the coarse grained beads according to the molecular weights of the hydrophilic and hydrophilic blocks.

As an input parameter for calculating the interaction between two beads, the solubility parameters of the beads were calculated using the Synthia module in the Materials Studio program package, based on the semi-empirical connectivity indices method. Additional detailed information about the mesoscale simulation procedure can be found in previous

studies by the present authors [44, 45]. In the present work, the time step and total number of steps were set to 50 ns and 3000, respectively. The noise parameter was set to 75.002, and the compressibility parameter was 10 kT. The grid parameter and total grid size were 1.0 nm and 36 × 36 × 36 nm, respectively. All mesoscale simulations were performed at 298 K.

3. Results and discussion

3.1. Synthesis of the hydrophilic (DSQFBP) and hydrophobic (BPS) oligomers

A new type of disulfonated fluorinated oligomer, DSQFBP, was designed to increase the acidity of the sulfonated group via the negative inductive effect of a fluorine-containing hydrophilic segment in the multiblock copolymer, as shown schematically in Figure 2a (Section 2.3). The ^{1}H-NMR and ^{19}F-NMR spectra of the starting materials and the novel hydrophilic oligomer are presented in Figures 3a and b. Thus, after the reaction of DSHQ with DFBP, the ^{1}H-NMR spectrum of DSQFBP reveals the disappearance of the H_b hydroxide peak at 9.75 ppm, along with a shift of the phenyl proton peak (H_a) from 6.81 ppm to 7.45 ppm due to the strong electron withdrawing effect of the fluorine atoms in DFBP. Moreover, a comparison of the ^{19}F-NMR spectra (Figure 3b) reveals the disappearance of the *para*-fluorine peak (F_c) of DFBP at around −150.01 ppm, along with a shift in the *meta*-fluorine peak (F_b) from around −161.01 ppm in the DFBP to −154.80 ppm in the DSQFBP due to the electron withdrawing effect of the disulfonated moieties in monomer (DSHQ). These phenomena confirm the successful synthesis of the DSQFBP oligomer.

Non-sulfonated biphenyl-based poly(arylene ether sulfone) oligomers (BPSs) with molecular weights of 5,000 and 10,000 g mol^{-1} were synthesized as hydrophobic segments in the multiblock copolymer. The structure of the hydrophobic BPS oligomer is confirmed by

the ^{1}H-NMR spectrum in Figure 3c [32].

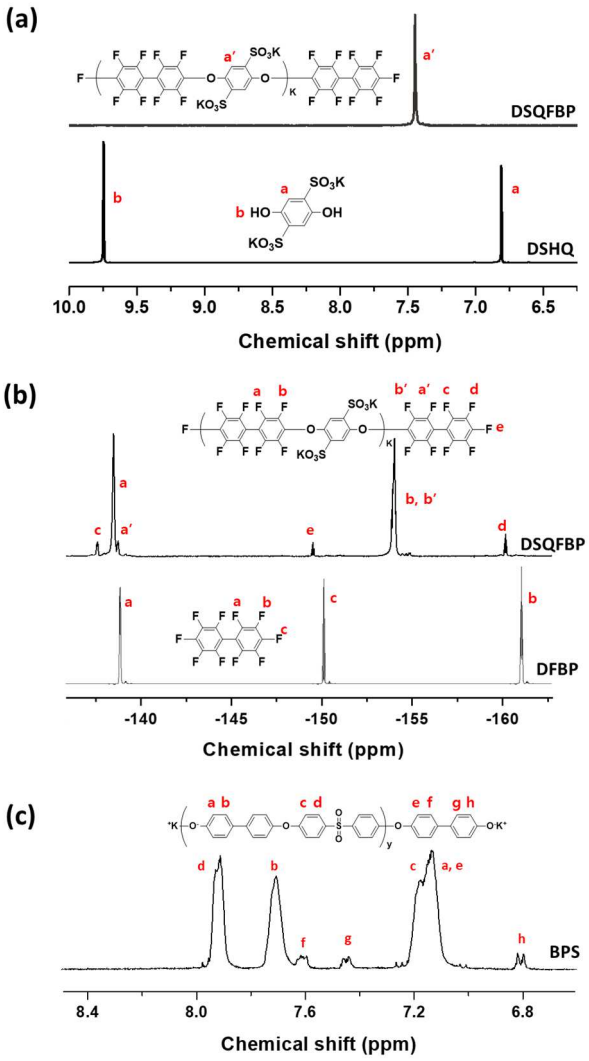

Figure 3. Proton (^{1}H) and fluorine (^{19}F) NMR analyses: (a) the ^{1}H-NMR spectra and (b) the ^{19}F-NMR spectra of the hydrophilic oligomer (DSQFBP) and the starting monomers (DSHQ and DFBP); (c) the ^{1}H-NMR spectrum of the hydrophobic oligomer.

The molecular weights of the hydrophilic and hydrophobic oligomers can be controlled by the monomer feed ratio [39]. The number-average molecular weights (M_n) of the DSQFBP and BPS oligomers were calculated by comparing the integrals of the end-group fluorine and proton peaks with those of the main chain fluorine and proton peaks. The determined M_n and measured intrinsic viscosity (IV) values of the oligomers are summarized in Table 1. Here,

the target and calculated molecular weights are nearly identical, thus confirming the successful synthesis of each oligomer. Furthermore, the log–log plots of M_n versus IV in Figure S1 indicate linear relationships for both the hydrophilic and hydrophobic oligomers (Table S1), thus confirming successful control of the molecular weight [32].

Table 1 The number average molecular weights (M_n) of the hydrophilic (DSQFBP) and hydrophobic (BPS) oligomers.

Oligomer Sample	Target M_n (g mol^{-1})	Measured M_n (g mol^{-1})[a]	IV (dL g^{-1})[b]
DSQFBP	10,000	10,600	0.15
BPS	5,000	4,900	0.20
	10,000	10,100	0.34

[a] Calculated from the relative ^{1}H and ^{19}F NMR integrals of the proton between the aromatic resonances.
[b] Measured at 60 °C in NMP with 0.05 M LiBr.

3.2. Synthesis of DSQFBP-BPS multiblock copolymers

The DSQFBP-BPS multiblock copolymer was synthesized by a coupling reaction between the phenoxide-terminated BPS oligomer and the DFBP-terminated DSQFBP oligomer, as depicted in Figure 2c (Section 2.3). The coupling reaction was conducted between the phenoxide end groups on the hydrophobic oligomer and the fluorine atoms on the hydrophilic oligomer. The successful coupling reaction is confirmed by the ^{1}H-NMR and ^{19}F-NMR spectra in Figures 4a and b, which reveal the disappearance of the proton peaks (H_e, H_f, and H_g) of the biphenyl end groups and the fluorine peak (F_e) at around −150.03 ppm, along with downfield shifts in the H_h and F_d peaks**.**

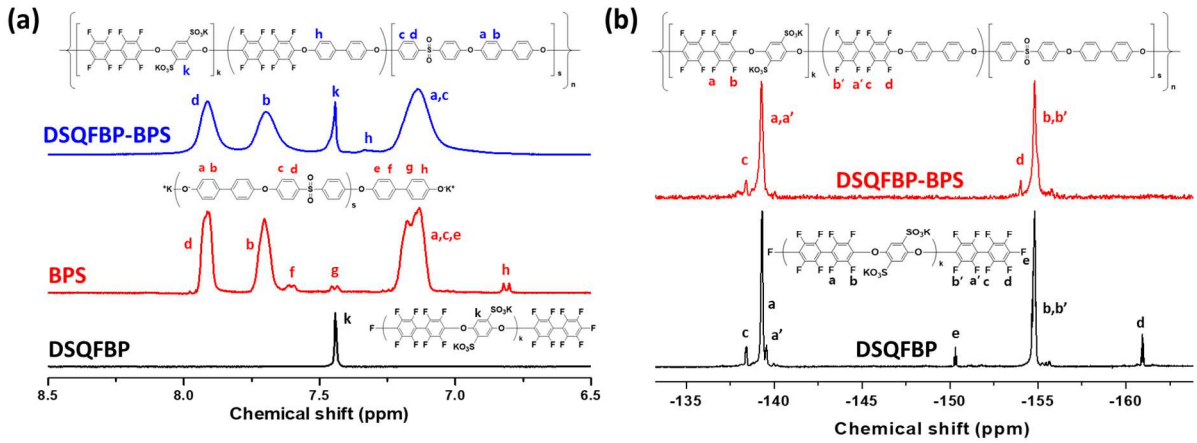

Figure 4. Proton (^{1}H) and fluorine (^{19}F) NMR analyses: (a) ^{1}H -NMR spectra and (b) ^{19}F -NMR spectra of the multiblock copolymer and the corresponding oligomers.

Figure 5. Images of two multiblock membranes prepared with different block ratios.

Table 2. The IV, MWD, IEC, water uptake, and swelling ratios of the multiblock copolymer, the BPSH40 and Nafion 212.

Samples	IV (dL g^{-1})[b]	MWD (M_n/M_w)	IEC (meq g^{-1})[c]		Water Uptake (weight%)[d]		Swelling Ratio (%)[e] Δl		Δt		Proton Conductivity (S cm^{-1})	
			Cald.	Exptl.	30 °C	90 °C	30 °C	90 °C	30 °C	90 °C	30 °C	90 °C
10k–5k[a]	1.67	3.24	2.19	2.00	96.8 ± 2.8	179.5 ± 3.0	14.5 ± 2.8	31.1 ± 2.9	79.4 ± 6.3	127.7 ± 5.4	0.289 ± 0.007	0.466 ± 0.008
10k–10k[a]	1.30	2.90	1.61	1.55	37.5 ± 3.1	63.7 ± 3.9	6.2 ± 2.3	14.3 ± 0.0	35.7 ± 6.5	46.0 ± 2.8	0.149 ± 0.005	0.347 ± 0.009
BPSH40	1.52	3.01	1.72	1.62	36.1 ± 2.0	58.2 ± 0.6	8.4 ± 2.2	21.0 ± 2.2	18.1 ± 1.3	27.4 ± 4.1	0.083 ± 0.002	0.216 ± 0.009
Nafion 212	--[f]	--[f]	--[f]	0.95–1.01[g]	17.6 ± 1.6	35.7 ± 2.5	10.5 ± 0.0	21.1 ± 0.0	9.5 ± 1.9	22.5 ± 3.0	0.136 ± 0.005	0.234 ± 0.005

[a] The hydrophilic–hydrophobic M_n is based on the K^+ form of the oligomer.
[b] Measured at 60 °C in NMP with 0.05 M LiBr.
[c] Measured using a classical titration method.
[d] Measured after immersion in deionized water at 30 °C for 48 h and at 90 °C for 5 h.
[e] Measured after immersion in deionized water at 30 °C for 48 h and at 90 °C for 5 h; Δl and Δt are the changes in the in-plane and through-plane directions, respectively.
[f] Cannot be measured.
[g] The average IEC of Nafion 212 as obtained from https://www.fuelcellstore.com/spec-sheets/nafion-211–212-spec-sheet.pdf.

3.3. The ion exchange capacities (IECs), water uptakes, swelling ratios, ion conductivities, and thermal stabilities of the membranes

Through the solvent casting method, two multiblock membranes were obtained as shown in Figure 5, which were pale yellow transparent and flexible. The measured IV and molecular weight distribution (MWD) values of the multiblock copolymers are listed, along with the transport properties of the various membranes (multiblock, random, and PFSA), in Table 2. The IEC values were obtained using a classical titration method. For the two multiblock membranes with different hydrophobic block lengths (i.e., 5k and 10k) and a fixed hydrophilic block (i.e., 10k), the hydrophilic ratio is seen to increase with decreasing hydrophobic block length. Accordingly, the IEC values of 10k–5k and 10k–10k are found to be 2.00 and 1.55 meq g^{-1}, respectively. Moreover, the BPSH40 random copolymer membrane exhibits an IEC value of 1.62 meq g^{-1}, which is similar to that of the 10k–10k multiblock

copolymer membrane.

In addition, the water uptakes and swelling ratios of the four membranes were measured at 30 and 90 °C and are given in Table 2. Here, the water uptake at 90 °C is seen to be 63.7 wt.% for the 10k–10k membrane, compared to a significantly higher 179.5 wt.% for the 10k–5k with the shorter hydrophobic block. The increased hydrophilicity of the 10k–5k leads to a higher IEC and, hence, a higher water content in the membrane. Moreover, despite having a slightly lower IEC, the 10k–10k multiblock membrane exhibits higher water uptakes of 37.5 and 63.7 wt.% at 30 and 90 °C, respectively, compared to 36.1 and 58.2 wt.%, respectively, for the BPSH40 random membrane. This is attributed to the presence of large hydrophilic ionic channels in the multiblock membrane, as indicated by the AFM images in Figure 7 (Section 3.4).

In contrast to their similar water uptakes, the 10k–10k and BPSH40 membranes exhibit significantly different in-plane and through-plane swelling ratios (Table 2). Nevertheless, both membranes exhibit a slightly lower swelling ratio in the in-plane direction compared to the through-plane direction. Thus, the swelling ratio of the 10k–10k at 90 °C is 14.3% in the in-plane direction and 46.0% in the through-plane direction, whereas those of the BPSH40 are 21.0% and 27.4%, respectively. This phenomenon is generally observed in multiblock membranes [32]. Further, in spite of a significantly increased water uptake of 179.5 wt.%, the swelling ratio of the 10k–5k membrane at 90 °C is 31.1% in the in-plane direction, which is an advantage when fabricating the device.

The proton conductivity is affected by the IEC, the interconnectivity of the hydrophilic ionic channels, and the acidity of the functional groups [24, 30, 34–36, 46]. As indicated in Figure 6, the 10k−10k and 10k−5k multiblock membranes exhibit proton conductivities at 90 °C that are, respectively, 1.48 and 1.99 times that of Nafion 212. Thus, the 10k–5k exhibits the

highest proton conductivity of 0.466 S cm^{-1} at 90 °C, which is primarily due to its higher IEC value of 2.0 meq g^{-1}. Further, despite a lower IEC and a similar water uptake to that of the BPSH40 membrane, the 10k–10k membrane exhibits a 60% higher proton conductivity of 0.347 S cm^{-1} at 90 °C compared to 0.216 S cm^{-1} for the latter. These results are explained by the enhanced acidity of the fluorinated sulfonated hydrophilic segment, which leads to suitable phase separation and well-formed ion channels, as revealed in Figure 7 (Section 3.4).

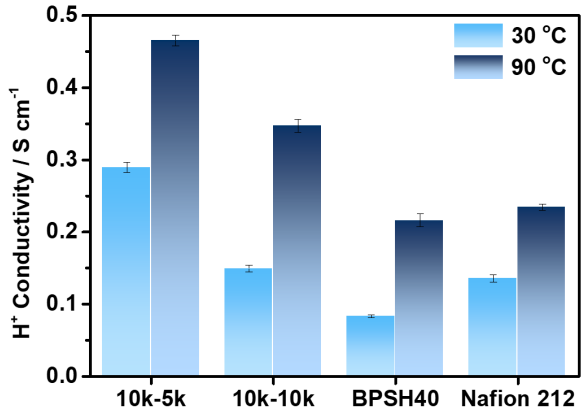

Figure 6. The proton conductivities of the multiblock (10k–5k and 10k–10k) membranes, a random membrane (BPSH40), and Nafion 212, at 30 °C and 90 °C.

The thermal decomposition and weight loss behavior of the 10k−5k, 10k−10k, and BPSH40 membranes are indicated by the TGA curves in Figure S2. Here, the initial weight loss represents the evaporation of residual solvent and water below 200 °C, while the second is due to degradation of the sulfonic acid groups at temperatures of up to 300 °C. Subsequently, decomposition of the polymer backbone begins at approximately 450 °C. Thus, although the 10k–5k and 10k–10k membranes exhibit fairly similar thermal degradation behaviors, the thermal stability of the latter is slightly higher due, primarily, to the presence of fewer sulfonic acid groups and, hence, a lower IEC. Nevertheless, the multiblock and BPSH40 membranes each exhibit sufficient thermal decomposition temperatures to operate even above

the 100 °C required for PEMWE.

3.4. Morphological analysis

The AFM phase images of the 10k−5k, 10k−10k, BPSH40, and Nafion 212 membranes are presented in Figure 7. Here, the dark regions indicate hydrophilic domains containing sulfonic acid groups with a large fraction of water, whereas the bright regions indicate the hydrophobic domains [24, 28, 47]. As noted above, the multiblock membranes (Figures 7a and b) exhibit superior phase separation between these hydrophilic and hydrophobic domains, along with an enhanced connectivity provided by well-defined nano-sized ionic channels like the Nafion 212 (Figure 7d), compared to the random copolymer (Figure 7c). Moreover, the 10k–5k membrane (Figure 7a) exhibits ionic channels of a wider hydrophilic domain width of 10–16 nm compared to that of 4.0–8.5 nm for the 10k–10k membrane (Figure 7b). By contrast, the BPSH40 exhibits no specific morphology due to the randomly substituted sulfonic acid groups along the poly(arylene ether sulfone) (PAES) backbone.

For the multiblock polymer membranes with a set hydrophilic length (i.e., 10k), the specific hydrophobic length (10k vs 5k) influences the transport properties. Thus, the larger the hydrophilic domains, the higher will be the water uptake of the membrane, thus providing well-defined ion channels even at a relative humidity below 40%. Consequently, the design of well-defined morphological structures by varying the block length is critical for controlling the transport properties of the membrane. These well-connected, wider hydrophilic domains result in increased proton conductivity and water retention [24].

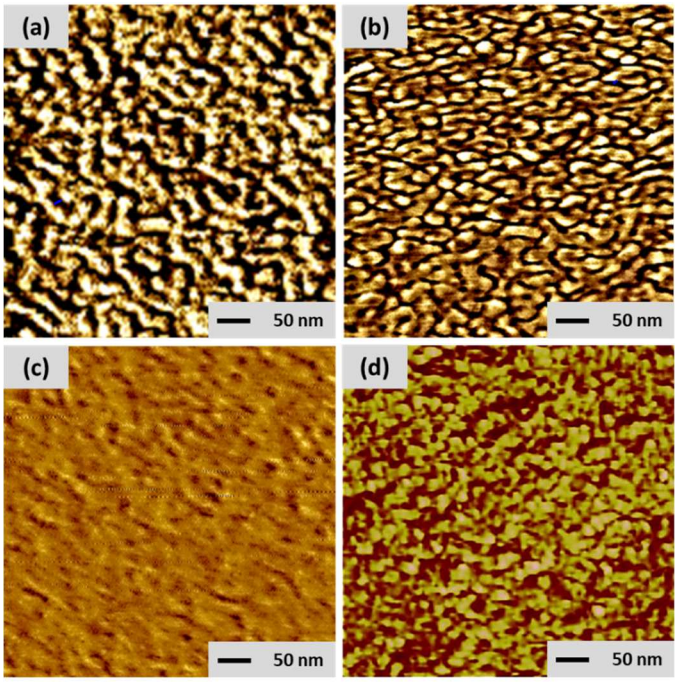

Figure 7. AFM images of (a) 10k–5k, (b) 10k–10k, (c) BPSH40, and (d) Nafion 212.

The result of the mesoscale simulation of the 10k−5k, 10k−10k, and BPSH40 membranes are presented in Figure 8. Here, the morphologies of the hydrophilic domains correspond closely to those observed in the above AFM images. Thus, the blue color in the simulated 10k–5k membrane indicates the presence of very strong, well-connected hydrophilic domains (Figure 8a), whereas the 10k–10k membrane exhibits relatively small, less well-connected domains (Figure 8b). Moreover, the absence of a phase-separated morphology is indicated in the simulated BPSH40 (Figure 8c). This simulation indicates that the higher the solubility parameters of each bead, the higher will be the polar-polar interactions and hydrophilicity. Note that the solubility parameter of the hydrophilic repeating unit in the BPSH40 (25.3 $(J/cm^3)^{1/2}$) is closely similar to that of the multiblock copolymers (25.1 $(J/cm^3)^{1/2}$). Moreover, the three membranes all have the same hydrophobic repeating unit, with a solubility parameter of 22.72 $(J/cm^3)^{1/2}$. This result indicates that while the phase-separated morphology in the multiblock has a significant impact on the transport behavior, it is the relative chain

length of the hydrophilic and hydrophobic segments that dictates the overall properties. Thus, even though the 10k–10k and 10k–5k copolymers have the same chemical structure of repeating units, the larger proportion of hydrophobic segments in the former can disrupt the strong inter-connectivity and cause the ensuing phase-separation of the hydrophilic block.

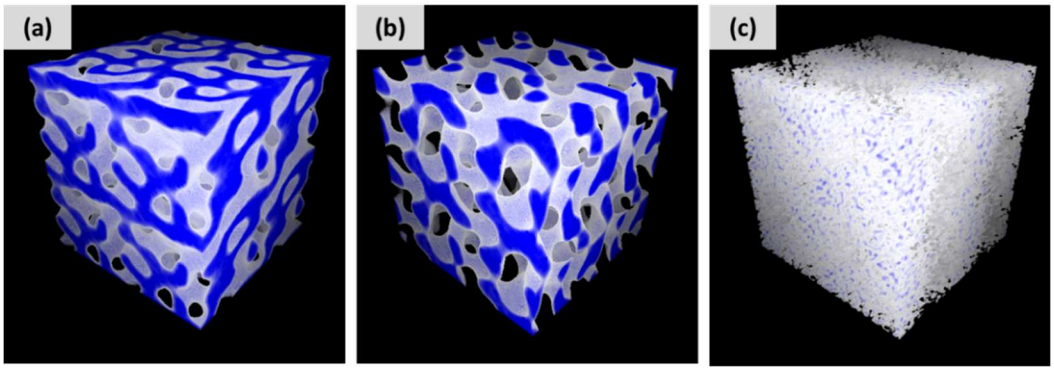

Figure 8. The simulated hydrophilic domains (blue) in (a) the 10k–5k membrane, (b) the 10k–10k membrane, and (c) the BPSH40 membrane.

3.5. Gas permeability

One of the critical roles of the PEM is to prevent each fuel from crossing over between the anode and cathode, with a low H_2 permeability leading to high WE efficiency and safety for long-term operation. The H_2 and O_2 gas permeabilities of the membranes are indicated in Figure 9a, where the Nafion 212 is seen to exhibit the highest value. Nevertheless, the multiblock membranes exhibit higher gas permeabilities for both H_2 and O_2 than does the BPSH40. Furthermore, both gas permeabilities are higher for the 10k–5k than for the 10k–10k, due primarily to the wider hydrophilic channels of the former membrane The morphology of the multiblock membranes clearly affect the gas permeability by facilitating the transport of ions, water, and gases [46]. Therefore, the hydrocarbon-based membranes reveal a trade-off between transport properties and gas permeability. The overall O_2 permeability values with respect to each condition are smaller because the kinetic diameter of

O_2 (3.46 Å) is larger than that of H_2 (2.89 Å) as shown in Figure 9a. In addition, as shown in Figure 9b, the gas permeability of all membranes at higher temperature was increased by one of the gas transport models, the solution-diffusion model [41]. The Nafion 212 has the highest H_2 permeability of 38.6 barrer than the multiblock membranes and BPSH40 at 90 °C. On the other hand, the hydrocarbon-based membranes showed less than half of the Nafion 212 with 16.9 barrer even for 10k–5k. Therefore, the developed multiblock membranes have the lower H_2 permeability than that of the commercial Nafion 212 membrane even at high temperature, so it is expected that efficient operation of PEMWE is possible.

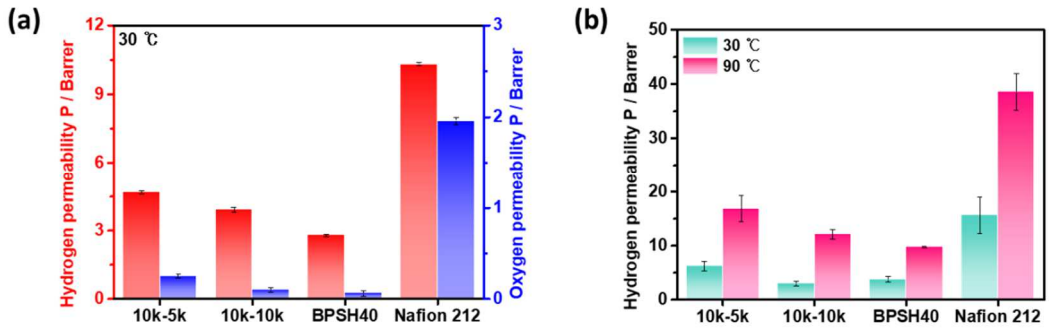

Figure 9. Gas permeability of the various membranes; (a) the hydrogen and oxygen permeability by the time-lag method at 30 °C, (b) the hydrogen permeability by the pressure decay method at 30 °C and 90 °C.

3.6. The WE performance

The WE performances of MEAs with the two types of multiblock membrane, the random BPSH40 membrane, and the commercial Nafion 212 membrane, are indicated in Figure 10. To obtain high-purity H_2 at the cathode, nothing was fed in, water was supplied only to the anode [48], and the WE performance was evaluated. A Nafion ionomer was used as the electrode binder for both the anode and cathode. The results in Figure 10 indicate a clear difference in the performance of the 10k–5k and 10k–10k membranes, with cell current

densities of 3.41 and 2.79 A cm^{-2}, respectively, at 1.9 V. By contrast, the BPSH40 exhibits the lowest proton conductivity and, hence, the lowest WE performance of 2.01 A cm^{-2} at 1.9 V due to the absence of a phase-separated morphology. Hence, the WE performances of the PEMs examined in the present study are proportional to the proton conductivities of each membrane, which are, in turn, influenced by their acidities and morphological properties. The WE performances of these membranes are further compared with those of various previously-reported hydrocarbon-based PEMs and PFSAs in Figure 1b [7–9, 14–18]. Here, the 10k–5k multiblock membrane exhibits an overwhelmingly superior WE performance due primarily to the effective proton transport provided by the long-range continuity of the ionic nano-channels in the multiblock membrane [46].

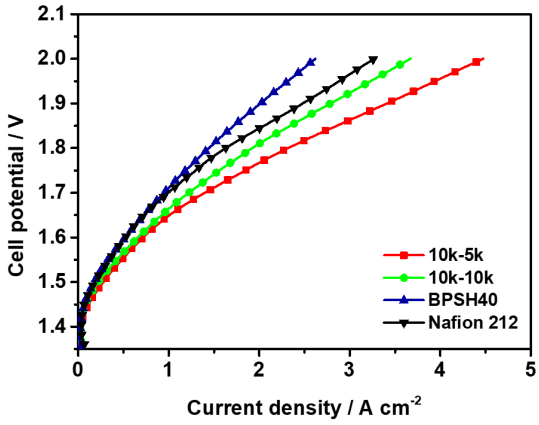

Figure 10. The WE performance of multiblock samples (10k–5k and 10k–10k), BPSH40, and Nafion 212 membranes.

4. Conclusions

Novel DSQFBP-BPS multiblock copolymers with high acidity and well-defined ion channels were synthesized via a coupling reaction between hydrophilic and hydrophobic segments and evaluated as potential PEMs for water electrolysis. The fluorinated sulfonated hydrophilic segment was designed to increase the acidity of sulfonic acid and produce a clear

distinction between the morphological effects of the hydrophilic and hydrophobic domains. The mechanism behind the improved performance of the multiblock membrane was elucidated via a comprehensive study on the effects of the morphological structure upon the transport properties and gas permeability of random and multiblock copolymers. Although the 10k–10k and BPSH40 membranes exhibited similar IEC and water uptake values, the former exhibited a 60% higher proton conductivity, thus resulting in a 40% enhancement in the WE performance, but the H_2 permeability of the 10k–10k membrane was increased by approximately 24% at 90 °C. Furthermore, the 10k–5k membrane, with its relatively shorter hydrophobic segment, exhibited the highest performance of 3.41 A cm^{-2} at 1.9 V due to the effective transport provided by the continuous nano-sized ionic channels. This result suggests that the creation of a morphology with wider ion channels and higher connectivity between the hydrophilic domains is critical to enhancing the WE performance. This conclusion was further supported by the mesoscale simulation data for the BPSH40, the 10k–5k, and the 10k–10k structures. These results indicate that the as-developed DSQFBP-BPS multiblock membranes provide a promising alternative PEM formulation for water electrolysis. However, further study is recommended in order to improve these DSQFBP-BPS multiblock membranes by optimizing their operating conditions and examining the effects of various system parameters.

Acknowledgments

This study was supported by the Hydrogen Energy Innovation Technology Development Program of the National Research Foundation of Korea (NRF) funded by the Korean government (MSIT) (No. 2019M3E6A1063674). This work was partially supported by the National Research Foundation of Korea (NRF) grant funded by the Korean government

(MSIT) (2019R1A2C1087209). This work was supported by the U.S. Department of Energy through the Los Alamos National Laboratory. Los Alamos National Laboratory is operated by Triad National Security, LLC, for the National Nuclear Security Administration of U.S. Department of Energy (Contract No. 89233218CNA000001).

References

[1] K. Mazloomi, C. Gomes, Hydrogen as an energy carrier: prospects and challenges, *Renew. Sust. Energ. Rev.* 16 (2012) 3024–3033.

[2] M. Carmo, D.L. Fritz, J. Mergel, D. Stolten, A comprehensive review on PEM water electrolysis, *Int. J. Hydrogen Energy* 38 (2013) 4901–4934.

[3] R. Maric, H. Yu, Proton exchange membrane water electrolysis as a promising technology for hydrogen production and energy storage, *Nanostructures in Energy Generation, Transmission and Storage,* IntechOpen (2019) 13.

[4] A. Kusoglu, A.Z. Weber, New insights into perfluorinated sulfonic-acid ionomers, *Chem. Rev.* 117 (2017) 987–1104.

[5] M.A. Hickner, H. Ghassemi, Y.S. Kim, B.R. Einsla, J.E. McGrath, Alternative polymer systems for proton exchange membranes (PEMs), *Chem. Rev.* 104 (2004) 4587–4612.

[6] H. Zhang, P.K. Shen, Recent development of polymer electrolyte membranes for fuel cells, *Chem. Rev.* 112 (2012) 2780–2832.

[7] D.W. Smith, F.O. Oladoyinbo, W.A. Mortimore, H.M. Colquhoun, M.S. Thomassen, A. Ødegård, N. Guillet, E. Mayousse, T. Klicpera, W. Hayes, A microblock ionomer in proton exchange membrane electrolysis for the production of high purity hydrogen, *Macromolecules* 46 (2013) 1504–1511.

[8] G. Wei, L. Xu, C. Huang, Y. Wang, SPE water electrolysis with SPEEK/PES blend membrane, *Int. J. Hydrogen Energy* 35 (2010) 7778–7783.

[9] V. Deimede, D. Labou, S.G. Neophytides, Polymer electrolyte membranes based on blends of sulfonated polysulfone and PEO-grafted polyethersulfone for low temperature water electrolysis, *J. Appl. Polym. Sci.* 131 (2014) 39922.

[10] A. Albert, A.O. Barnett, M.S. Thomassen, T.J. Schmidt, L. Gubler, Radiation-grafted polymer electrolyte membranes for water electrolysis cells: evaluation of key membrane properties, *ACS Appl. Mater. Interfaces* 7 (2015) 22203–22212.

[11] A. Daryaei, G.C. Miller, J. Willey, S.R. Choudhury, B. Vondrasek, D. Kazerooni, M.R. Burtner, C. Mittelsteadt, J.J. Lesko, J.S. Riffle, J.E. McGrath, Synthesis and membrane properties of sulfonated poly (arylene ether sulfone) statistical copolymers for electrolysis of water: Influence of meta-and para-substituted comonomers, *ACS Appl. Mater. Interfaces* 9 (2017) 20067–20075.

[12] I.-Y. Jang, O.-H. Kweon, K.-E. Kim, G.-J. Hwang, S.-B. Moon, A.-S. Kang,

Covalently cross-linked sulfonated poly (ether ether ketone)/tungstophosphoric acid composite membranes for water electrolysis application, *J. Power Sources* 181 (2008) 127–134.

[13] R.S.L. Yee, R.A. Rozendal, K. Zhang, B.P. Ladewig, Cost effective cation exchange membranes: A review, *Chem. Eng. Res. Des.* 90 (2012) 950–959.

[14] M.-A. Song, S.-I. Ha, D.-Y. Park, C.-H. Ryu, A.-S. Kang, S.-B. Moon, J.-H. Chung, Development and characterization of covalently cross-linked SPEEK/Cs-TPA/CeO_2 composite membrane and membrane electrode assembly for water electrolysis, *Int. J. Hydrogen Energy* 38 (2013) 10502–10510.

[15] J.E. Park, J. Kim, J. Han, K. Kim, S. Park, S. Kim, H.S. Park, Y.-H. Cho, J.-C. Lee, Y.-E. Sung, High-performance proton-exchange membrane water electrolysis using a sulfonated poly (arylene ether sulfone) membrane and ionomer, *J. Membr. Sci.* 620 (2021) 118871.

[16] J.E. Park, S. Kim, O.-H. Kim, C.-Y. Ahn, M.-J. Kim, S.Y. Kang, T.I. Jeon, J.-G. Shim, D.W. Lee, J.H. Lee, Y.-H. Cho, Y.-E. Sung, Ultra-low loading of IrO_2 with an inverse-opal structure in a polymer-exchange membrane water electrolysis, *Nano Energy* 58 (2019) 58–166.

[17] V.K. Puthiyapura, S. Pasupathi, H. Su, X. Liu, B. Pollet, K. Scott, Investigation of supported IrO_2 as electrocatalyst for the oxygen evolution reaction in proton exchange membrane water electrolyser, *Int. J. Hydrogen Energy* 39 (2014) 1905–1913.

[18] J. Park, Z. Kang, G. Bender, M. Ulsh, S.A. Mauger, Roll-to-roll production of catalyst coated membranes for low-temperature electrolyzers, *J. Power Sources* 479 (2020) 228819.

[19] K.-S. Lee, M.-H. Jeong, J.-P. Lee, J.-S. Lee, End-group cross-linked poly (arylene ether) for proton exchange membranes, *Macromolecules* 42 (2009) 584–590.

[20] K.-S. Lee, M.-H. Jeong, J.-S. Lee, B.S. Pivovar, Y.S. Kim, Optimizing end-group cross-linkable polymer electrolytes for fuel cell applications, *J. Membr. Sci.* 352 (2010) 180–188.

[21] M. Sumner, W.L. Harrison, R.M. Weyers, Y.S. Kim, J.E. McGrath, J.S. Riffle, A. Brink, M.H. Brink, Novel proton conducting sulfonated poly (arylene ether) copolymers containing aromatic nitriles, *J. Membr. Sci.* 239 (2004) 199–211.

[22] L. Fu, H. Liao, G. Xiao, D. Yan, Sulfonated poly (arylene ether)s with high content of phosphine oxide moieties for proton exchange membranes, *J. Membr. Sci.* 389 (2012) 407–

415.

[23] S. Matsumura, A.R. Hlil, C. Lepiller, J. Gaudet, D. Guay, A.S. Hay, Ionomers for proton exchange membrane fuel cells with sulfonic acid groups on the end groups: Novel linear aromatic poly (sulfide− ketone)s, *Macromolecules* 41 (2008) 277–280.

[24] M.L. Einsla, Y.S. Kim, M. Hawley, H.-S. Lee, J.E. McGrath, B. Liu, M.D. Guiver, B.S. Pivovar, Toward improved conductivity of sulfonated aromatic proton exchange membranes at low relative humidity, *Chem. Mater.* 20 (2008) 5636–5642.

[25] H.-S. Lee, A. Roy, O. Lane, S. Dunn, J.E. McGrath, Hydrophilic–hydrophobic multiblock copolymers based on poly (arylene ether sulfone) via low-temperature coupling reactions for proton exchange membrane fuel cells, *Polymer* 49 (2008) 715–723.

[26] K. Yoshimura, K. Iwasaki, Aromatic polymer with pendant perfluoroalkyl sulfonic acid for fuel cell applications, *Macromolecules* 42 (2009) 9302–9306.

[27] K. Matsumoto, T. Higashihara, M. Ueda, Locally and densely sulfonated poly (ether sulfone)s as proton exchange membrane, *Macromolecules* 42 (2009) 1161–1166.

[28] K.-S. Lee, M.-H. Jeong, J.-P. Lee, Y.-J. Kim, J.-S. Lee, Synthesis and characterization of highly fluorinated cross-linked aromatic polyethers for polymer electrolytes, *Chem. Mater.* 22 (2010) 5500–5511.

[29] Q. Li, Y. Chen, J.R. Rowlett, J.E. McGrath, N.H. Mack, Y.S. Kim, Controlled disulfonated poly (arylene ether sulfone) multiblock copolymers for direct methanol fuel cells, *ACS Appl. Mater. Interfaces* 6 (2014) 5779–5788.

[30] A.S. Badami, O. Lane, H.-S. Lee, A. Roy, J.E. McGrath, Fundamental investigations of the effect of the linkage group on the behavior of hydrophilic–hydrophobic poly (arylene ether sulfone) multiblock copolymers for proton exchange membrane fuel cells, *J. Membr. Sci.* 333 (2009) 1–11.

[31] H. Ghassemi, J.E. McGrath, T.A. Zawodzinski Jr, Multiblock sulfonated–fluorinated poly (arylene ether)s for a proton exchange membrane fuel cell, *Polymer* 47 (2006) 4132–4139.

[32] H.-S. Lee, O. Lane, J.E. McGrath, Development of multiblock copolymers with novel hydroquinone-based hydrophilic blocks for proton exchange membrane (PEM) applications, *J. Power Sources* 195 (2010) 1772–1778.

[33] H.S. Lee, A. Roy, O. Lane, M. Lee, J.E. McGrath, Synthesis and characterization of multiblock copolymers based on hydrophilic disulfonated poly (arylene ether sulfone) and hydrophobic partially fluorinated poly (arylene ether ketone) for fuel cell applications, *J.*

Polym. Sci. A: Polym. Chem. 48 (2010) 214–222.

[34] Y.A. Elabd, M.A. Hickner, Block copolymers for fuel cells, *Macromolecules* 44 (2011) 1–11.

[35] Y. Chang, G.F. Brunello, J. Fuller, M. Hawley, Y.S. Kim, M. Disabb-Miller, M.A. Hickner, S.S. Jang, C. Bae, Aromatic ionomers with highly acidic sulfonate groups: acidity, hydration, and proton conductivity, *Macromolecules* 44 (2011) 8458–8469.

[36] Y. Chang, G.F. Brunello, M. Disabb-Miller, M. Hawley, Y.S. Kim, M.A. Hickner, S.S. Jang, C. Bae, Poly (arylene ether sulfone) ionomers with different acidity strengths and fuel cell membrane properties, *ECS Transactions* 50 (2013) 1031–1035.

[37] Ionization constants of heteroatom organic acids, https://www2.chemistry.msu.edu/faculty/reusch/VirtTxtJml/acidity2.htm.

[38] F. Wang, M. Hickner, Y.S. Kim, T.A. Zawodzinski, J.E. McGrath, Direct polymerization of sulfonated poly (arylene ether sulfone) random (statistical) copolymers: candidates for new proton exchange membranes, *J. Membr. Sci.* 197 (2002) 231–242.

[39] G. Odian, Principles of Polymerization, Third Ed., John Wiley & Sons. Inc.: New York 1991.

[40] J. Yang, Y. Li, A. Roy, J.E. McGrath, Viscometric behavior of disulfonated poly (arylene ether sulfone) random copolymers used as proton exchange membranes, *Polymer* 49 (2008) 5300–5306.

[41] S.H. Kim, B.T.D. Nguyen, H. Ko, M. Kim, K. Kim, S.Y. Nam, J.F. Kim, Accurate evaluation of hydrogen crossover in water electrolysis systems for wetted membranes, *Int. J. Hydrogen Energy* 46 (2021) 15135–15144.

[42] J.G.E.M. Fraaije, Dynamic density functional theory for microphase separation kinetics of block copolymer melts, *J. Chem. Phys.* 99 (1993) 9202–9212.

[43] J.G.E.M. Fraaije, B.A.C van Vlimmeren, N.M. Maurits, M. Postma, O.A. Evers, C. Hoffmann, P. Altevogt, G. Goldbeck-Wood, The dynamic mean-field density functional method and its application to the mesoscopic dynamics of quenched block copolymer melts, *J. Chem. Phys.* 106 (1997) 4260–4269.

[44] C.H. Park, S.Y. Lee, C.H. Lee, Investigation of water channel formation in sufonated polyimides via mesoscale simulation, *Membrane J.* 27 (2017) 389–398.

[45] N. Li, C. Wang, S.Y. Lee, C.H. Park, Y.M. Lee, M.D. Guiver, Enhancement of proton transport by nanochannels in comb-shaped copoly (arylene ether sulfone)s, *Angew. Chem.* 123 (2011) 9324–9327.

[46] D.W. Shin, M.D. Guiver, Y.M. Lee, Hydrocarbon-based polymer electrolyte membranes: importance of morphology on ion transport and membrane stability, *Chem. Rev.* 117 (2017) 4759–4805.

[47] Y.S. Kim, M.A. Hickner, L. Dong, B.S. Pivovar, J.E. McGrath, Sulfonated poly (arylene ether sulfone) copolymer proton exchange membranes: composition and morphology effects on the methanol permeability, *J. Membr. Sci.* 243 (2004) 317–326.

[48] M.K. Cho, H.-Y. Park, H.J. Lee, H.-J. Kim, A. Lim, D. Henkensmeier, S.J. Yoo, J.Y. Kim, S.Y. Lee, H.S. Park, J.H. Jang, Alkaline anion exchange membrane water electrolysis: Effects of electrolyte feed method and electrode binder content, *J. Power Sources* 382 (2018) 22–29.

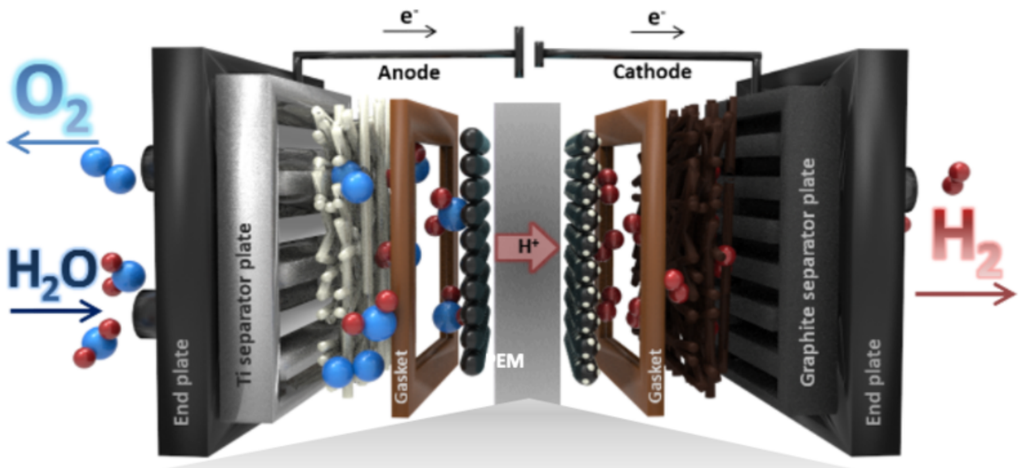

Hydrocarbon based copolymer

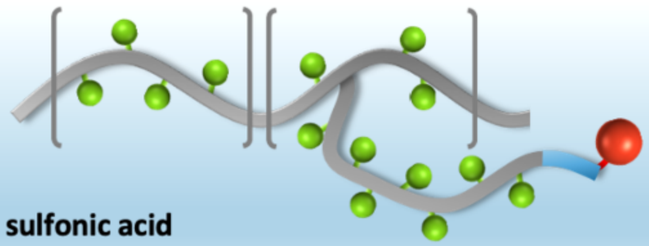

Perfluorinated sulfonic acid

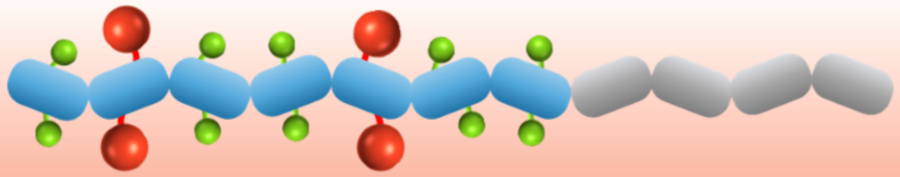

Multiblock with enhanced hydrophilic block

Fluorine $SO_3^-H^+$ Hydrophilic Hydrophobic